Korea-Australia Rheology Journal
Vol. 21, No. 1, March 2009 pp. 71-79

Transient filling simulations in unidirectional fibrous porous media

Hai Long Liu and Wook Ryol Hwang*
School of Mechanical and Aerospace Engineering, Research Center for Aircraft Parts Technology (ReCAPT), Gyeongsang National University, Gajwa-dong 900, Jinju, South Korea
(Received October 30, 2008; final revision received March 2, 2009)

Abstract

The incomplete saturation and the void formation during the resin infiltration into fibrous porous media in the resin transfer molding process cause failure in the final product during its service. In order to better understand flow behavior during the filling process, a finite-element scheme for transient flow simulation across the micro-structured fibrous media is developed in the present work. A volume-of- fluid (VOF) method has been incorporated in the Eulerian frame to capture the evolution of flow front and the vertical periodic boundary condition has been combined to avoid unwanted wall effect. In the microscale simulation, we investigated the transient filling process in various fiber structures and discussed the mechanism leading to the flow fingering in the case of random fiber distribution. Effects of the filling pressure, the shear-thinning behavior of fluid and the volume fraction on the flow front have been investigated for both intra-tow and the inter-tow flows in dual-scale fiber tow models.

Keywords : resin transfer molding, transient infiltration, finite element method, volume-of-fluid method

1. Introduction

The capability of manufacturing high performance structured composite materials at relatively low operation cost made the resin transfer molding (RTM) process an attractive technique in aerospace, transport and automotive industries (Bader, 2001). In the RTM filling processing, either thermosetting or thermoplastic polymer is injected to infuse a fiber preform that is placed in closed mold. In most cases, the fiber preform is fabricated or stitched in various architectures from fiber tows, which are bundles of hundreds of parallel fiber filaments, to ensure that the fiber content in composite product could be enough to carry the mechanical loads. Such a fiber preform could be described as dual-scales porous medium, since the gaps between fiber tows are of the order of millimeters whereas the interstices between fiber filaments inside the fiber tows are of the order of micrometers. Accordingly, under normal filling pressure, the resin fills the intra-tow region between the fiber tows at a much faster rate than inter-tow region within the fiber tows. On the other hand, the random arrangement of fiber filament in micro scale results in a non-uniformed impregnation. As a consequence, poor saturation and voids might be present in final parts, which possibly cause the initiation of cracks during their service (Varna *et al.*, 1995). Hence understanding of the underlying physical phenomena during fluid impregnation through a fibrous preform is of great importance for the industry applications.

A number of previous works on the transient filling during the RTM process can be found in literatures. In many cases, the resin transportation into the fiber preform is modeled by the standard Darcy's law (Bruschke and Advani, 1990; Kang and Lee, 1999; Mohan *et al.*, 1999). Although these approaches were found to be successful in tracking the flow front in the macroscopic flow, they are incapable to give any information about the fiber tow saturation or the air entrapment inside the fiber tow. Pillai *et al.* (2002) proposed to add the 'sink term' in the momentum equation to account for the resin impregnation into the fiber tow in dual scale porous media. According to this modification, Simacek and Advani (2003) introduced extra one dimensional element into the standard finite-element/control-volume scheme to represent the saturation of fiber tows. The saturation rate of the fiber tow is assumed to be linearly proportional to the pressure of the macro flow in the inter-tow region. Though simplified, the model was somewhat successful in predicting the partially saturated region qualitatively.

Several researchers have investigated the impregnation of fiber tow in meso-scale for transverse and longitudinal flows. Both Sadiq *et al.* (1995) and Parnas *et al.* (1994) demonstrated that the transverse flow is always delayed by the viscous resistance of the fiber tow, even though there exists strong capillary effect between individual fiber filaments inside the fiber tow. To some extent, for the flow

*Corresponding author: wrhwang@gsnu.ac.kr

transverse to the fiber array, the hydrodynamic force seems to be more dominant, when the filling pressure is larger than the capillary pressure. Spaid and Phelan (1998) modeled the transverse flow though fiber tow using the Lattice Boltzmann (LB) method, which showed time-dependent saturation profile inside the fiber tow and investigated void formation dynamics as a function of the nominal porosity. Chang (2003) also proposed a model to simulate coupled flows in both intra-tow and inter-tow spaces and they showed that the mechanism of air entrapment formed inside the fiber bundles is caused by non-homogeneous spatial distribution of permeability. Binetruy *et al.* (1997) investigated the axial flow along the fiber tow and proposed the mathematic model to predict the position of delayed flow front in intra-tow region as a function of efficient and saturated permeability. Even without considering the capillary force in modeling the flow inside the fiber tow, their result shows good agreement with experiment at high volume content. Yang *et al.* (2006) modeled a similar problem and employed a volume-of-fluid method to observe the flow front along the fiber tow in dual scale porous media. The effects of intra-tow permeability, filling velocity and inter-tow dimension on flow front have been studied.

In the present study, we track the flow front by the volume-of-fluid (VOF) method based on the finite element scheme. In micro-scale simulations, we present flow patterns for randomly distributed fiber array and investigate the mechanisms leading to the flow fingering. In meso-scale simulations, a fiber tow model is presented to investigate non-homogeneity in the flow front between the intra-tow and the inter-tow flows, which is believed to be responsible for the poor saturation or void formation inside the fiber tow. Effects of the filling pressure, the amount of shear-thinning in fluid, the viscosity, fiber volume fraction and the inter-tow dimension on the saturation profiles have been studied.

2. Modeling

2.1. Problem definition

In this work, the transversal flow crossing a porous media is modeled as the flow through the unidirectional fiber filaments with the circular cross section. By distributing fiber filaments in desired configurations, we could mimic the fiber bed with various microstructures, including the dual-scale model of fiber tows. Fig. 1 describes the resin impregnation into the fiber tow driven by the pressure, which is an example of the flow in dual-scale porous media.

The computational domain in the present work is given in Fig. 2. The Cartesian x and y coordinates are selected as parallel and normal to the flow direction. The computational domain, denoted by Ω, has four boundaries, which

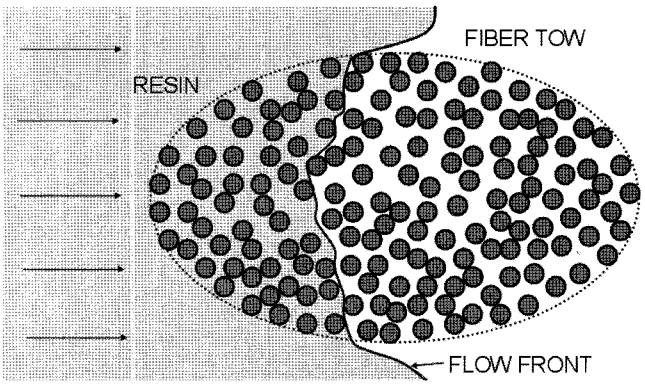

Fig. 1. The transversal impregnation inside the fiber tow during the filling process.

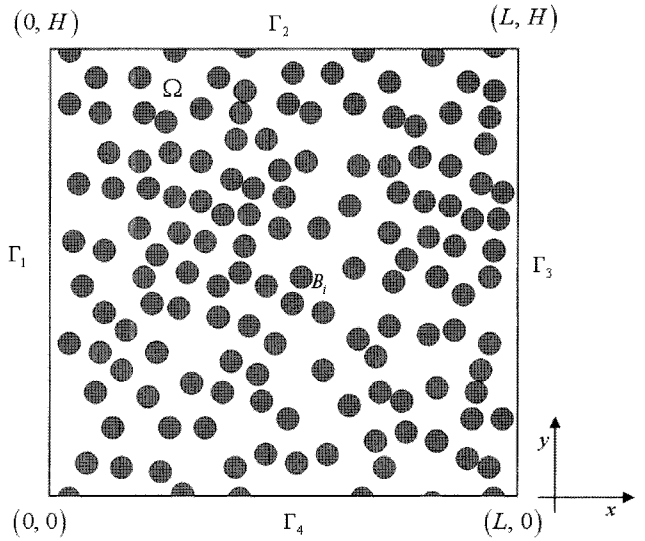

Fig. 2. The computational domain with the combination of periodic boundary condition to the vertical direction.

are denoted by $\Gamma_i (i=1, 2, 3, 4)$. The fiber filament is denoted by B_i $(i=1, 2, 3..., N)$ and N is the number of fibers. We used the symbol B to denote a collective region occupied by the fiber. In our model, the constant pressure injection condition is imposed on the inlet to drive the fluid flow passively crossing the fiber array. In addition, the periodic boundary condition has been introduced between the upper (Γ_2) and lower (Γ_4) boundaries in y direction. The periodic boundary condition in the vertical direction allows a more flexible way to arrange fibers such that the fibers could be located crossing the upper or lower boundary, avoiding the unwanted wall effect in mold filling simulation.

In the present study, we focus on the hydrodynamic effects on the micro-scale filling in the porous media, neglecting the capillary effect, since the capillary effect only works dominantly when the local pressure is extremely low (Wang and Grove, 2008; Dungan and Sas-

try, 2002). In the case of practical manufacturing processes, the filling pressure is normally chosen high enough to make sure the filling stage could be finished before resin starting to cure. Therefore, the flow induced by capillary force could not be very significant during the transient filling stage.

2.2. Governing set of equations

The governing equations for Stokes flow of a generalized Newtonian fluid are employed to describe the transversal flow through micro fiber arrays.

$$\nabla \cdot \sigma = 0, \text{ in } \Omega \backslash B \tag{1}$$

$$\nabla \cdot \boldsymbol{u} = 0, \text{ in } \Omega \backslash B \tag{2}$$

$$\sigma = -p\boldsymbol{I} + 2\eta_{fluid}(\dot{\gamma})\boldsymbol{D}, \text{ in } \Omega \backslash B \tag{3}$$

Eqs. (1)-(3) are for the momentum balance, the continuity, the constitutive relation, and the symbols $\boldsymbol{u}$, σ, p, $\boldsymbol{I}$, $\boldsymbol{D}$ and η are the velocity, the stress, the pressure, the identity tensor, the rate-of-deformation tensor and the viscosity, respectively. The shear rate $\dot{\gamma} = (2\boldsymbol{D}:\boldsymbol{D})^{1/2}$ is the second invariant of $2\boldsymbol{D}$ in the complex flow. The (truncated) power-law model is employed to express the shear-rate dependent viscosity in case of a non-Newtonian fluid:

$$\eta_{fluid}(\dot{\gamma}) = m\dot{\gamma}^{n-1}. \tag{4}$$

In this model, a limiting low shear rate $\dot{\gamma}_{ref}$ has been introduced such that the shear rate smaller than $\dot{\gamma}_{ref}$ is replaced by $\dot{\gamma}_{ref}$ to avoid unrealistic high viscosity in the low shear regime The fluid attached on the fiber B_i must be stationary:

$$\boldsymbol{u} = \boldsymbol{0}, \text{ on } \partial B_i. \tag{5}$$

In addition, the flow is driven by the pressure gradient between inlet and outlet:

$$p(0,y) - p(L,y) = \Delta p \tag{6}$$

A fictitious domain method (Wang and Hwang, 2008; Hwang *et al.*, 2004; Glowinski *et al.*, 1999; Bertrand *et al.*, 1997) has been implemented to describe the fiber filaments in our model. In this method, the fiber is considered as an immobilized rigid ring, which is filled with the same fluid as in the fluid domain and the zero velocity condition is imposed only along the fiber boundary. It is called the rigid-ring problem and it was introduced for the simulation of particle suspensions by Hwang *et al.* (2004), and Hwang and Hulsen (2006). This description is possible when fluid inertia is negligible. The governing equations for a region occupied by a fiber B_i are exactly the same as equations for the fluid domain in Eqs. (1)-(3). Therefore, the additional condition for the fiber is the zero velocity constraint on the fiber boundary, as indicated in Eq. (5).

The interface between the fluid and air was captured by the pseudo-concentration method, proposed by Haagh and Van De Vosse (1998). This method is well suited with the rigid-ring description for the fiber with the fictitious domain method, since both methods are based on the Eulerian description with a fixed regular mesh over the entire domain. In the pseudo-concentration method, the fluid and air are identified by the concentration function f, indicating the fraction of fluid materials: *i.e.*, $\phi = 0$ for the air domain, while $\phi = 1$ for the fluid domain. The interface is determined by the level set $\phi = 0.5$. The fraction of material should be advected passively by the given flow and therefore the evolution of the concentration function ϕ is given as follows:

$$\frac{\partial \phi}{\partial t} + \boldsymbol{u} \cdot \nabla \phi = 0 \tag{7}$$

In the frame work of the pseudo-concentration method, the viscosity is now denoted by η^* over the entire domain:

$$\eta^* = \phi\eta_{fluid} + (1-\phi)\eta_{air}. \tag{8}$$

We use a constant air viscosity η_{air} of order 10^{-3} to minimize the artificial effect of air domain on the fluid flow. Then, the constitutive relation for both fluid and air is given by a single equation:

$$\sigma = -p\boldsymbol{I} + 2\eta^*(\dot{\gamma}, \phi)\boldsymbol{D} \tag{9}$$

Since the periodic boundary condition has been applied in the vertical direction, the continuity of the velocity field and of the concentration function and the force balance are required across the periodic boundary:

$$\boldsymbol{u}(0,y) = \boldsymbol{u}(L,H), \ \phi(0,y) = \phi(L,H), \ \boldsymbol{t}(0,y) = -\boldsymbol{t}(L,H), \ x \in [0,L], \tag{10}$$

where $\boldsymbol{t}$ are tractions on the domain boundary.

When the fiber is located across the periodic boundaries, it needs to be relocated into the computational domain to

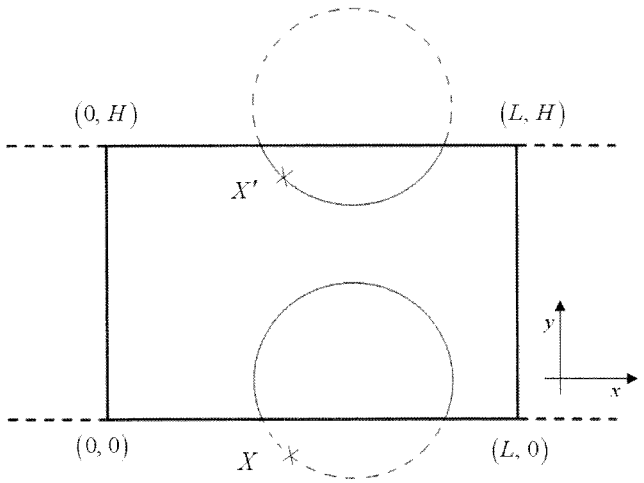

Fig. 3. The description of a fiber crossing the periodic boundary in the vertical direction. The part of a fiber exceeds the upper or lower boundary of computational domain has been relocated.

the corresponding position as indicated in Fig. 3. We define two sets of the coordinates: the unprimed set for the original coordinate (before relocation) and the primed set for the relocated coordinate. The relocated coordinate (x',y') is determined by

$$x' = x,\ y' = \mathrm{mod}(y,H) \tag{11}$$

where 'mod' is the modular function: *e.g.*, $\mathrm{mod}(1.7Y,H) = 0.7Y$ and $\mathrm{mod}(-0.7Y,H) = 0.3Y$ for the positive number Y.

3. Numerical methods

Following the approach in the previous work for the permeability prediction (Wang and Hwang, 2008), we derive the weak form and the discontinuous Galerkin (DG) method is employed in weak form to get the stable solution of the interface evolution equation (Eq. (7)). We introduce two different Lagrangian multipliers λ^v and $\lambda^{B,i}$, which are associated with the kinematical constraints for the periodicity in the vertical direction (Eq. (10)) and the rigid-ring constraint equation along the i-th fiber filament boundary, respectively:

$$\lambda^v = (\lambda_x^v, \lambda_y^v) \in L^2(\Gamma_3),\ \lambda^{B,i} = (\lambda_x^{B,i}, \lambda_x^{B,i}) \in L^2(\partial B_i) \tag{12}$$

Introducing the separate functional spaces U, P and Φ for $\boldsymbol{u}$, p and ϕ, respectively, the weak form over the entire domain, along with the DG formulation for the evolution equation, can be stated as follow:

For $t>0$, find $\boldsymbol{u} \in U$, $p \in \mathrm{P}$, $\phi \in \Phi$, $\lambda^v \in L^2(\Gamma_4)$ and $\lambda^{B,i} \in L^2(\partial B_i)$ such that:

$$-\int_\Omega p\nabla\cdot v d\Omega + \int_\Omega 2\eta^*(\dot\gamma)\boldsymbol{D}[\boldsymbol{u}]\boldsymbol{D}[\boldsymbol{v}]d\Omega + (\lambda^v, v(x,H)-v(x,0))_{\Gamma_4}$$

$$+\sum_{i=1}^{N}(\lambda^{B,i}, v)_{\partial B_i} = -\int_{\Gamma_1}\Delta p(\boldsymbol{n},\boldsymbol{v})d\Omega, \tag{13}$$

$$\int_\Omega q\nabla\cdot u d\Omega = 0, \tag{14}$$

$$\int_\Omega \psi\left(\frac{\partial\phi}{\partial t} + \boldsymbol{u}\cdot\nabla\phi\right)d\Omega - \sum_e \int_{\Gamma_e^{\mathrm{in}}}\psi(\phi-\phi^{\mathrm{ext}})(\boldsymbol{u}\cdot\boldsymbol{n}_e)ds = 0, \tag{15}$$

$$(\mu^{B,i}, \boldsymbol{u})_{\partial B_i} = 0,\ (i=1,...,N), \tag{16}$$

$$(\mu^v, \boldsymbol{u}(x,0)-v(x,H))_{\Gamma_4} = 0 \tag{17}$$

for all $v \in U$, $q \in \mathrm{P}$, $\psi \in \Phi$, $\mu^v \in L^2(\Gamma_4)$ and $\mu^{B,i} \in L^2(\partial B_i)$. In Eq. (15), $\boldsymbol{n}_e$ is the unit outward normal vector on the boundary of an element e, Γ_e^{in} is the part of the boundary e where $\boldsymbol{u}\cdot\boldsymbol{n}_e<0$ and ϕ^{ext} is the concentration in the neighboring upwind element. The inner product $(\cdot,\cdot)_{\Gamma_j}$ is the standard inner product in $L^2(\Gamma_j)$:

$$(\mu, v)_{\Gamma_j} = \int_{\Gamma_j}\mu\cdot v ds.$$

We remark that when a fiber is located outside the periodic domain, the part beyond the domain needs to be relocated according to Eq. (11). In this case, Eqs. (13) and (16) should be modified as follow:

$$(\mu^{B,i}(x'), u(x'))_{\partial B_i} = 0 \tag{18}$$

In a similar way, the inflow condition of the concentration function (Eq. (10)) has been incorporated for the flow front crossing the periodic boundary with the DG formulation (Eq. (15)) by taking the coupled position of the periodic boundary.

4. Implementation

4.1. Spatial discretization

For the discretization of the weak form, we use quadrilateral elements over the whole domain with the bi-quadratic interpolation of the velocity, the linear discontinuous interpolation for the pressure and discontinuous bi-quadratic interpolation of the concentration function. For the discretization of the weak form of the rigid-ring constraint (Eqs. (13) and (16)), we employ the point collocation method and details of implementation technique can be found in Wang and Hwang (2008) and Hwang *et al.* (2004). Presented in Fig. 4 is an example mesh for three fiber filaments. In order to keep the flow rate, we employed more collocation points for each fiber boundary than in the particle suspension simulation (Hwang *et al.*, 2004). For the vertical periodicity (Eq. (17)), we used nodal collocation method, the point collocation at all nodes along the periodic boundary.

4.2. Time integration

At the initial time step, we set the concentration function to be zero over the whole computational domain as no

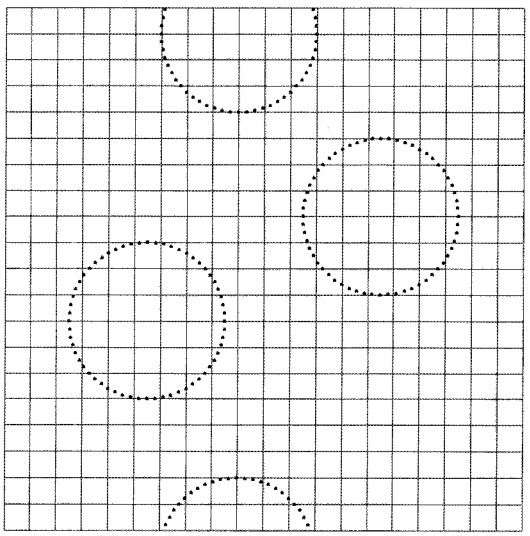

Fig. 4. The regular rectangular discretization is used for the entire computational domain and the fiber is described by the collocation points along its boundary.

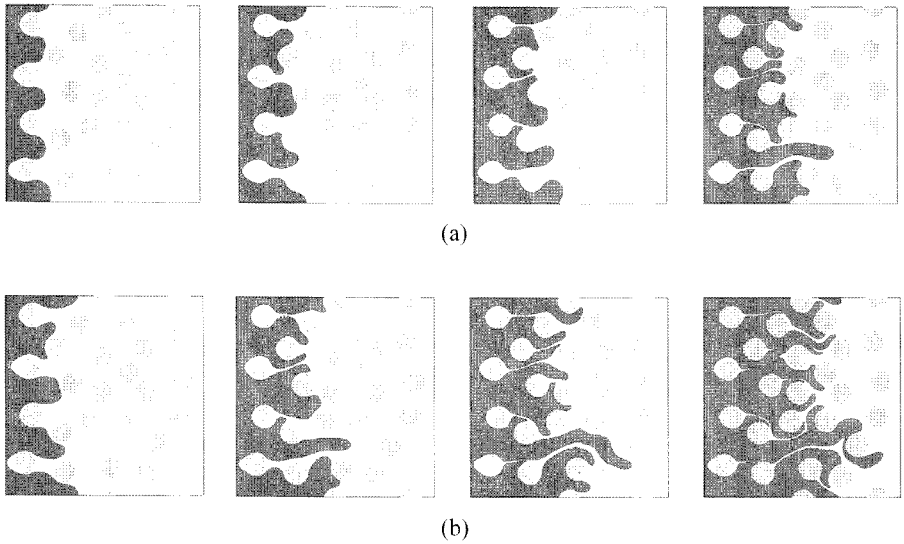

Fig. 5. The flow front evolution through 25 random distributed fibers at $t=0.2$, 0.5, 1 and 2 for each case (a): Newtonian fluid, (b): non-Newtonian fluid with power-law index $n=0.5$.

fluid filled inside. At following each time steps, we solve the momentum equation with the constraints of the rigid ring and the periodicity (Eqs. (13), (14), (16), (17)) to get the velocity distribution $\boldsymbol{u}^n$, then we predict the concentration function (ϕ^{n+1}) by integrating the evolution equation of the concentration function equation (Eq. (15)) from $\boldsymbol{u}^n$. As the accuracy of the interface capture really depends on the accuracy of the time-stepping method, we employ the explicit third-order accurate TVD-RK3 (Total-Variance_diminshing/3rd−order Runge-Kutta) scheme combined with discontinuous Galerkin method:

$$[M]\left(\frac{\tilde{\phi}^{n+1}-\phi^n}{\Delta t}\right)=\boldsymbol{g}(\boldsymbol{u}^n,\phi^n),$$

$$[M]\left(\frac{\tilde{\phi}^{n+2}-\tilde{\phi}^{n+1}}{\Delta t}\right)=\boldsymbol{g}(\boldsymbol{u}^n,\tilde{\phi}^{n+1}),\ \tilde{\phi}^{n+0.5}=\frac{1}{4}(3\phi^n+\tilde{\phi}^{n+2}),$$

$$[M]\left(\frac{\tilde{\phi}^{n+1.5}-\tilde{\phi}^{n+0.5}}{\Delta t}\right)=\boldsymbol{g}(\boldsymbol{u}^n,\tilde{\phi}^{n+0.5}),$$

$$\phi^{n+1}=\frac{1}{3}(\phi^n+2\tilde{\phi}^{n+1.5}), \tag{19}$$

where $[M]$ is the mass matrix and vector $\boldsymbol{g}$ is the forcing term due to the convection term in the evolution equation of ϕ.

During solving the governing equations mentioned above, we need to solve a large symmetric sparse matrix. We use a direct method based on a sparse multi-frontal variant of Gaussian elimination (HSL/MA41) to solve the matrix system. Additionally, the Picard-type iteration has been employed to deal with the non-linearity in the non-Newtonian fluid problem.

5. Results and discussion

5.1. Micro-scale flow simulations

In this section we investigate the flow pattern in the unidirectional fiber bed of randomly packed fiber filaments for both Newtonian and shear-thinning fluids. For this purpose, the first problem is set up with 25 randomly distributed fibers of the uniform radius r = 0.0275 in the computational domain of the size $(L,H)=(0.5,0.5)$ under the pressure drop $\Delta p=50$. Figs. 5(a) and (b) show the flow front evolution at $t=0.2$, 0.5, 1, 2 for a Newtonian fluid with the viscosity $\eta_{fluid}=1$ and for a shear-thinning fluid with $m=1$ and $n=0.5$, respectively. In both cases, the interfaces get wiggling in time, which indicates the non-uniform infiltration. Such phenomena, so called the 'interface fingering', appear more evident in the shear-thinning fluid case. The long advancement of the interface is caused by the local acceleration of the interface velocity through the gap between two adjacent fibers. This acceleration was also reported by Chen and Papathanasiou (2006) in their steady flow simulation for unidirectional randomly distributed fiber media. Moreover, one could observe a long tail of voids for each fiber boundary on the downstream, after the flow passes by the fiber. The void structure is very similar to the meld line formation in the injection molding process. Though there is no experimental evidence of this void formation right after the microscale fiber filament, it seems to be largely affected by the distance between the adjacent fibers in the flow direction. However, detailed analysis of the flow front near the fiber needs to be carried out in the future with full consideration of the interfacial contact wetting phenomenon.

As mentioned previously, the non-uniformity of the inter-

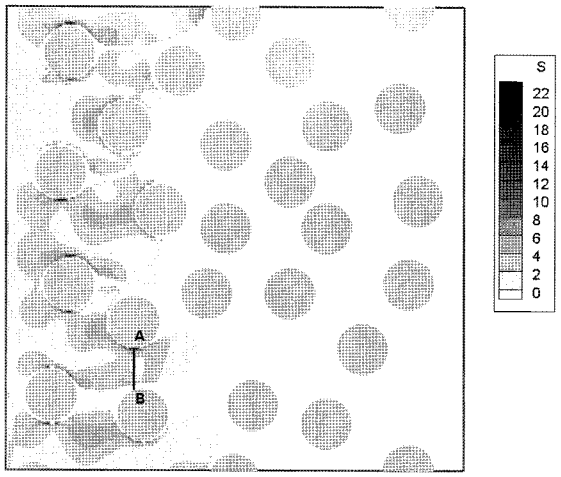

(a)

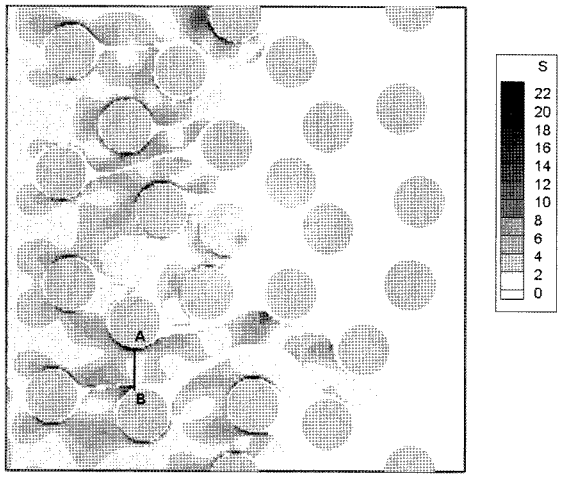

(b)

Fig. 6. The shear rate distribution at $t=1$. (a) Newtonian fluid. (b) shear-thinning fluid with the power-law index $n=0.5$.

face in the shear-thinning fluid is more evident than in a Newtonian fluid. To investigate the enhanced fingering in case of the shear-thinning fluid, the shear-rate distributions at $t=1$ for both cases are presented in Fig. 6, since the shear rate is a dominant fact that leads to variations in the shear-thinning fluid. As shown in Fig. 6(b), the high shear region appears near the top and the bottom of the fiber boundaries, where the fingering of the flow front is enhanced. (See the line segment denoted by A-B.) In the high shear region, the velocity gradient is large, because the viscosity gets low due to the shear-thinning property. Therefore, one may expect the flow along the line segment A-B would be a plug flow. The result is consistent with the enhanced main flow path generation in the shear-thinning fluid in Wang and Hwang (2008).

To investigate the enhanced fingering in the shear-thinning fluid, we plotted in Fig. 7 the shear rate along the line

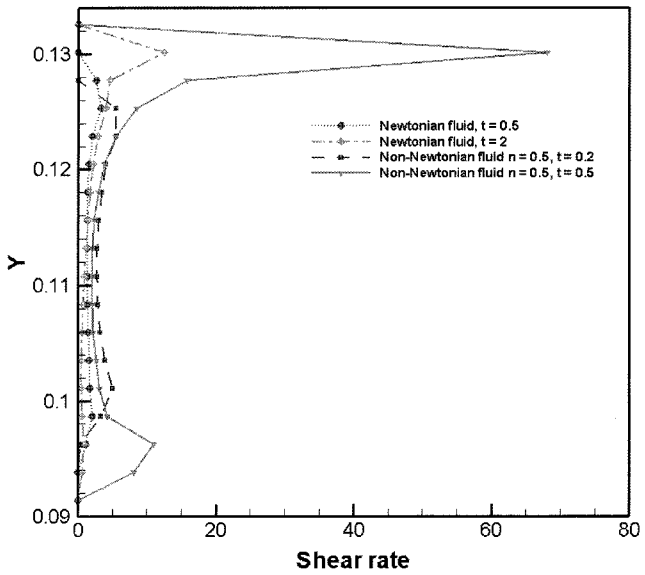

Fig. 7. The shear rate distribution along the line A-B (Fig. 6) between the two adjacent fibers on the boundary of the interface fingering at $t=0.2$ and 0.5 for a Newtonian fluid and at $t=0.5$ and 2 for a shear-thinning fluid.

A-B (denoted in Fig. 6). We compared the shear rate at $t=0.5$ and 2 in case of the Newtonian fluid and $t=0.2$ and 0.5 for the shear-thinning fluid, when the flow pattern is similar to each other. In Fig. 7, one could observe that the shear rate close to the fiber boundary is much higher in the non-Newtonian fluid than in the Newtonian one, which indicate the local plug-like flow formation near the gap and thereby it enhances the fingering of the flow front in case of the shear-thinning fluid.

5.2. Dual-scale flow simulations

As mentioned, the fiber preform is usually fabricated from fiber tows, which are bundles of hundreds of parallel fiber filaments, to ensure that the fiber content in the composite product could be enough to carry the mechanical loads. The flow in the fiber tow can be modeled as the dual-scale porous medium: the gaps between fiber tows are of the order of millimeters, whereas the interstices between fiber filaments inside the fiber tows are of the order of micrometers. Therefore the void formation due to the difference in the resin infiltration speed has been an important industrial issue. In the present study, we model an elliptic fiber bundle consisting of 107 fiber filaments with the uniform radius $r=0.02$ in the computational domain $(L,H)=(1.5,0.7)$ so that the dual-scale flow behaviors of the macro flow around the fiber tow as well as the micro flow inside the tow could be investigated in our simulation. We remark that, due to the periodicity in the vertical direction, the problem with a single fiber tow could represent the parallel arrays of fiber tow in the vertical direction.

Firstly, we investigate effects of the pressure gradient on

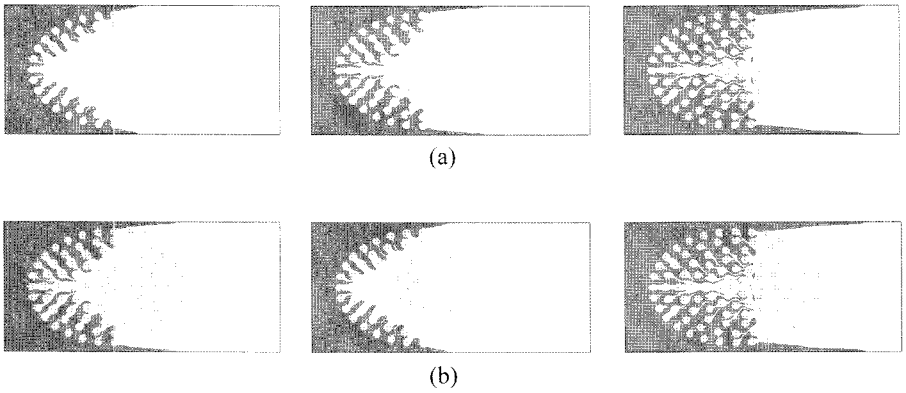

Fig. 8. The flow pattern through a fiber tow in a Newtonian fluid (a) at t=50, 100 and 300 with the pressure drop Δp=1; (b) at t=5, 10 and 30 with the pressure drop Δp=10.

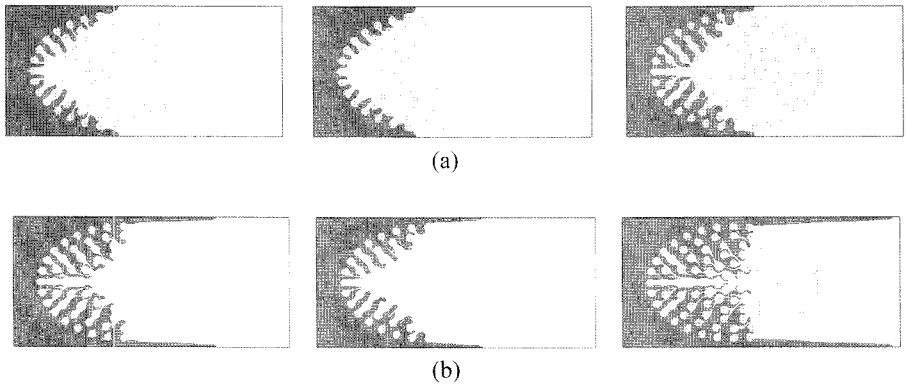

Fig. 9. The flow front evolutions in a dual scale media for a shear-thinning fluid with the power-law index n=0.5 (a) at t=50, 100 and 300 with the pressure drop Δp=1; (b) at t=5, 10 and 30 with the pressure drop Δp=10.

the saturation of fiber tow for a Newtonian fluid with η_{fluid}=1. The evolutions of the flow fronts in both macro- and micro-region at t=50, 100 and 300 under the pressure drop Δp=1 and at t=5, 10 and 30 under Δp=10 are presented in Fig. 8(a) and 8(b), respectively. The flow front in the macro gap of the inter-tow region (at the top and bottom of fiber tow) always advances ahead of that of the micro flow inside fiber tow and the distance between two interface, called the lagged distance, increases in time during the transient filling process. The lagged distance between two different scaled flows could be a criterion to evaluate the amount of incomplete filling and the potential of void formation. In this study, due to the assumption of Stokes flow, the flow field appears completely linear and the evolution of flow front is found to be linearly dependent on the pressure drop Δp, by comparing flow patterns at t=50, 100 and 300 under the pressure drop Δp=1 in Fig. 8(a) and the saturation profiles at t=5, 10 and 30 under Δp=10 in Fig. 8(b). In this regard, the result in Fig. 8 may show the accuracy of the code developed in the present study.

Secondly we considered the shear-thinning behavior of the fluid, by setting the power-law parameters n=0.5 and m=1, to investigate the effect of the pressure gradient under the same filling condition as in the previous Newtonian fluid. Plotted in Figs. 9(a) and 9(b) are the filling patterns at t=50, 100 and 300 under the pressure drop Δp=1 and at t=5, 10 and 30 under Δp=10, respectively. In comparison with Fig. 8(a) of the Newtonian fluid at the same time step, the flow front advancement under the low pressure drop is found slower in the shear thinning fluid in both intra-tow and inter-tow regions and the lagged distance between these macro and micro flows has been greatly reduced. On the other hand, with the high pressure drop Δp=10 in Fig. 9(b), the intra-tow flow inside the fiber tow has been found faster than in the lower pressure drop case and, at the same time, the inter-tow flow appears even faster. Thus, the lagged distance is found to increase under the high pressure gradient. The lowered viscosity under the high pressure drop (high shear rate) is responsible for the enhanced saturation in Fig. 9(b).

Next, the viscosity effect on the saturation of the fiber tow were investigated for the Newtonian fluid under the pressure drop Δp=10 with η_{fluid}=1, 0.6 and 0.2. From the

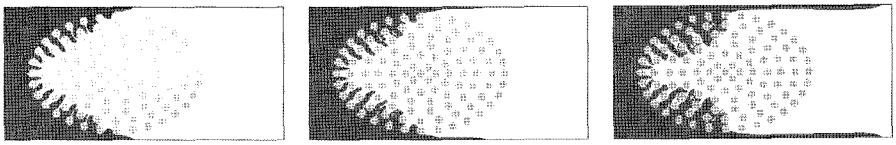

$\eta_{fluid}=1$ $\eta_{fluid}=0.6$ $\eta_{fluid}=0.2$

Fig. 10. The flow front evolution in a dual scale media at $t=4$ in a Newtonian fluid under the pressure drop $\Delta p=10$ with different viscosities $\eta_{fluid}=1$, 0.6 and 0.2.

flow patterns shown in Fig. 10, the lagged distance between the two different scaled flows became larger with the decreasing viscosity, although the decreased viscosity accelerates the flow advancement in inter-tow and intra-tow regions, which is quite similar to those occurring in case of the shear-thinning fluid under the high pressure drop. In the lowest viscosity case of $\eta_{fluid}=0.2$, the void would be most possibly formed inside the fiber tow, as the macro flow moves to the downstream much faster than the micro flow penetrating into the fiber tow.

To investigate the effect of the fiber fraction inside the fiber tow on the saturation behavior, we tested two fiber volume fractions ϕ_f of 12.8% ($r=0.02$, Fig. 11(a)) and 7.2% ($r=0.015$, Fig. 11(b)) under the pressure drop $\Delta p=10$ in a Newtonian fluid with $\eta_{fluid}=1$. As shown in Fig. 11, the fiber tow with the lower fiber content shows easier saturation inside the fiber tow, while the inter-tow flow front remains almost the same. As a consequence, the lagged distance decreases in the media with the lower fiber content, which agrees well with the simulation results of Spaid and Phelan (1998) with the lattice Boltzmann method.

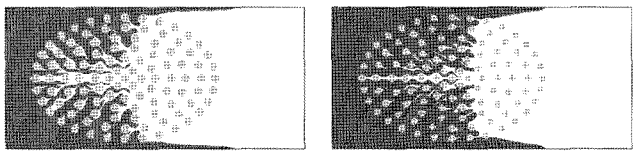

(a) (b)

Fig. 11. The flow front evolution in the dual scale media at $t=20$ of Newtonian fluid under the pressure drop $\Delta p=10$ for two different fiber volume fractions (a) $\phi_f=12.8\%$; (b) $\phi_f=7.2\%$.

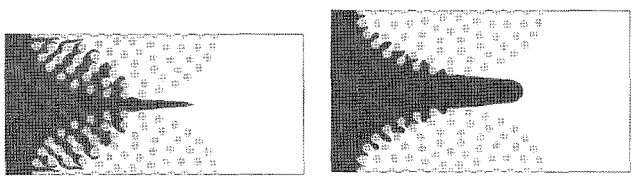

(a) (b)

Fig. 12. The flow front evolutions through fiber tow at $t=10$ in a Newtonian fluid under the pressure drop $\Delta p=10$ for two different inter-tow dimensions (a) in the computational domain $(L,H)=(1.5,0.7)$ at $t=10$; (b) $(L,H)=(1.5,0.8)$ at $t=2$.

Finally, effects of the inter-tow dimension on the saturation of the fiber tow was investigated in a Newtonian fluid with $\eta_{fluid}=1$. Plotted in Figs. 12(a) and 12(b) are the interface evolutions under the pressure drop $\Delta p=10$ in the computational domain $(L,H)=(1.5,0.7)$ at $t=10$ and $(L,H)=(1.5,0.8)$ at $t=2$, respectively. The vertical gap between the fiber tows is increased by 0.1 in Fig. 12(b). The increase in the inter-tow dimension causes the less infiltration into fiber tow (intra-tow flow), while the macro inter-tow flow front appears almost the same. The results presented in Figs. 11 and 12 indicates that the infiltration characteristics of a dual scale fiber preform cannot be simply determined from the fiber volume fraction, but the microstructures such as the fraction of the fiber filament in the fiber tow and the inter spacing between the fiber tow should be taken into consideration, besides the processing parameters like the fluid rheology and the pressure drop.

6. Conclusions

In this work, the transient transverse flow behaviors through unidirectional fibrous porous media have been studied numerically. Based on the finite-element method, we tracked the flow front using a volume-of-fluid method and the fixed fibers are described by the rigid ring problem with the fictitious domain method. In addition, the vertical periodic boundary condition has been introduced to avoid wall effects.

We observed the non-uniform filling in the microstructure with randomly distributed fibers and, more specifically, reported the formations of the interface fingering and of local tails of the void along the fiber boundary in the downstream. We found that the interface fingering phenomenon can be enhanced in a shear-thinning fluid due to local high shear regions in the vicinity of the fiber, introducing a plug-like flow, which is quite similar to the mechanism in the main flow path generation in a shear-thinning fluid in randomly distributed fiber arrays. We confirmed this argument by comparison of the local shear-rate distribution in Newtonian and shear-thinning fluids.

We performed meso-scale flows simulation for the fiber tow to understand the inter-tow and intra-tow flow char-

acteristics that is largely responsible for incomplete filling in the RTM process. Using a fiber tow consisting of 107 fibers in a vertically periodic domain, we investigated effects of the pressure drop, the amount of shear-thinning in a fluid, the viscosity, the porosity the gap distance between the tows on the dual-scale flow and, more specifically, on the appearance of the lagged distance, the distance between flow fronts for both inter-tow and intra-tow flows. In our simulation with a specific geometry of fiber tows, we observed that the lagged distance would increase with the low fluid viscosity, the high volume fraction and the large inter-tow gap by increasing the lagged distance between the two flows. The effect of the shear-thinning viscosity was found to depend strongly on the pressure drop: the high pressure drop enhances the intra-tow flow inside the fiber tow, but at the same time the inter-tow flow becomes even faster and thereby the lagged distance has been found to increase.

The present work demonstrates the feasibility to investigate the microscale transient flow behavior in fibrous arrays of various microstructures. The present scheme could be a useful tool in predicting the incomplete filling and void formation, which are quite important problems in the industrial liquid molding process. In the future, we will extend our scheme to incorporate the surface wetting effect between the fiber and fluid and make comparisons with the experimental results.

Acknowledgement

This work was supported by Korea Research Foundation Grant by the Korean government (KRF-2008-005-J01001).

References

Bader M. G., 2001, Polymer composites in 2000: structure, performance, cost and compromise, *Journal of Microscopy* **201**, 110-121.

Bertrand F., P. A. Tanguy and F. A. Thibault, 1997, A three-dimensional fictitious domain method for incompressible fluid flow problems, *International Journal of Numerical Methods in Fluids* **25**, 719-736.

Binetruy C., B. Hilaire and J. Pabiot, 1997, The interactions between flows occurring inside and outside fabric tows during RTM, *Composite Science and Technology* **57**, 587-596.

Bruschke M. V. and S. G. Advani, 1990, A finite element/control volume approach to mold filling in anisotropic porous media, *Polymer Composites* **11**, 398-405.

Chang C. Y., 2003, Tow impregnation of unidirectional fibrous perform during resin transfer molding, *Journal of Reinforced Plastics and Composites* **22**, 1003-1016.

Chen X. and T. D. Papathanasiou, 2006, On the variability of the Kozeny constant for saturated flow across unidirectional disordered fiber arrays, *Composites Part A* **37**, 836-846.

Dungan F. D. and A. M. Sastry, 2002, Saturated and unsaturated polymer flows: microphenomena and modeling, *Journal of Composites Materials* **36**, 1581-1603.

Glowinski R., T.-W Pan., T. I. Hesla and D. D. Joseph, 1999, A distributed Lagrange multiplier/fictitious domain method for particulate flows, *International Journal of Multiphase Flow* **25**, 755-794.

Haagh G. A. A. V. and F. N. Van De Vosse, 1998, Simulation of three-dimensional polymer mould filling processes using a peseudo-concentration method, *International Journal of Numerical Methods in Fluids* **28**, 1355-1369.

Hwang W. R., M. A. Hulsen and H. E. H. Meijer, 2004, Direct simulation of particle suspensions in sliding bi-periodic frames, *Journal of Computational Physics* **194**, 742-772.

Hwang W. R. and M. A. Hulsen, 2006, Direct numerical simulations of hard particle suspensions in planar elongational flow, *Journal of Non-Newtonian Fluid Mechanics* **136**, 167-178.

Kang M. K. and W. I. Lee, 1999, A flow-front refinement technique for the numerical simulation of the resin-transfer molding process, *Composite Science and Technology* **59**, 1663-1674.

Mohan R. V., N. D. Ngo and K. K. Tamma, 1999, On a pure finite-element-based methodology for resin transfer mold filling simulations, *Polymer Engineering and Science* **39**, 26-43.

Parnas R. S., A. J. Salem, T. A. K. Sadiq, H. Wang and S. G. Advani, 1994, The interaction between micro- and macroscopic flow in RTM performs, *Composite Structure* **27**, 93-107.

Pillai K. M., 2002, Governing equations for unsaturated flow through woven fiber mats. Part 1. Isothermal flows, *Composites: Part A* **33**, 1007-1019.

Sadiq T. A. K, S. G. Advani and R. S. Parnas, 1995, Experimental investigation of transverse flow through aligned cylinders, *International Journal of Multiphase Flow* **21**, 755-774.

Simacek P. and S. G. Advani, 2003, A numerical model to predict fiber tow saturation during liquid composite molding, *Composite Science and Technology* **63**, 1725-1736.

Spaid M. A. A. and F. R. Phelan, 1998, Modeling void formation dynamics in fibrous porous media with the lattice Boltzmann method, *Composites: Part A* **29A**, 749-755.

Varna J., R. Joffe and L. A. Berglund, 1995, Effect of voids on failure mechanisms in RTM laminates, *Composite Science and Technology* **53**, 241-249.

Wang Y. and S. M. Grove, 2008, Modelling microscopic flow in woven fabric reinforcements and its application in dual-scale resin infusion modeling, *Composites: Part A* **39**, 843-855.

Wang J. F. and W. R. Hwang, 2008, Transverse mobility prediction of non-Newtonian fluids across fibrous porous media, *Journal of Composite Materials*, submitted.

Wang J. F. and W. R. Hwang, 2008, Permeability prediction of fibrous porous media in a bi-periodic domain, *Journal of Composite Materials* **42**, 909-929.

Yang J., Y. Jia, S. Sun, D. Ma, T. Shi and L. Jia, 2006, Mesoscopic simulation of the impregnating process of unidirectional fibrous preform in resin transfer molding, *Materials Science and Engineering A*, **435-436**, 515-520.

Instructions for Authors

A. Submission of manuscripts

1. Manuscripts for the Korea-Australia Rheology Journal should be submitted to one of the two editors. The addresses of the editorial offices are as follows:
   • Professor Hyungsu Kim, Editor
   The Korean Society of Rheology
   Suite 806, The Korea Science and Technology Center
   635-4, Yuksam-dong, Gangnam-goo
   Seoul 135-703, Korea
   • Professor Ravi Prakash Jagadeeshan
   Department of Chemical Engineering
   Monash University
   Building 69, Room 213, Clayton Campus
   Melbourne ,VIC 3800, Australia
2. All work should be original and not have been previously published in any journal, book, or peer reviewed compilation. Those intending to write a review should first contact one of the editors. Letters to the Editor, book reviews and meeting/course announcements are also accepted subject to editorial review.

B. Manuscript preparation

1. All manuscripts must be prepared in English.
2. Manuscripts should be submitted in triplicate, typed double-spaced throughout and on one side of the paper only. Paper size should be 210 mm×297 mm (A4) or 8 1/2 in ×11 in (Letter) with margins of at least 25 mm on all sides.
3. The content should be ordered as follows: title, author name(s), affiliations and addresses including the e-mail address of the corresponding author, abstract (not exceeding 20 typewritten lines), keywords, text, acknowledgments, list of symbols, references, appendices, figure captions, tables. The abstract should be a summary of the whole paper, not the conclusions alone. The text should be reasonably subdivided into sections and subsections.
4. References should be cited in the text, using author(s), and the year of publication; for example, prior work by Kim (1994), by Boger and Walters (1997), and by Roh and co-workers (1995). Both authors are cited when there are two and the phrases and co-workers or *et al.* are employed to cite a publication having more than two authors. The references are compiled at the end of the manuscript in alphabetical order of the first author and arranged as follows:

   Kim, C., 1994, Collapse of spherical bubbles in Maxwell fluids, *J. Non-Newt. Fluid Mech.* **55**, 37-58.
   Boger, D.V. and K. Walters, 1993, Rheological Phenomena in Focus, Elsevier, Amsterdam.

5. Mathematical and chemical symbols, equations and formulae should be typed. All equations must be numbered sequentially in Arabic numerals in parentheses on the right-hand side of the page.
6. Authors are required to use the International System of Units (SI Unit) and their standard abbreviations where possible.
7. Illustrations must be original drawings or sharp black and white prints. Details of notation such as subscripts and superscripts, as well as labels and numbers on figure axes, must be legible after reproduction in A4 sheet. Computer graphics files must be submitted after the paper is accepted in the case of halftone art, shaded figures and figures in gray scale. Graphics must be submitted as BMP, PCX, PostScript, TIF or GIF. All figures must be numbered consecutively and referred to in the text. Captions for all figures must be compiled on a separate sheet. If figures are taken from copyrighted material, it is understood that the author has obtained permission from the copyright holder for their reproduction. Color illustrations can be reproduced at the author's expense. The author should contact one of the editorial offices for details.

C. Referees

Every paper is subject to peer-review. Authors may suggest suitable referees for their paper, although the editors reserve the right not to approach them.

D. Queries

Queries regarding accepted papers should be addressed to the editor to which the paper was submitted. All other queries (proofs or offprints) should be addressed to the Korean editorial office, or to Hyungsu Kim, The Korean Society of Rheology (E-mail:hkim@dku.edu).

E. Offprints and reprints

The corresponding author will receive 10 offprints of the paper and one copy of the journal free of charge. Extra copies of offprints, minimum 10, can be ordered by submitting a form (which is available upon request) to the Korean editorial office.